An Analytical Flow Model for PTFE Paste through Annular Dies

Pramod D. Patil, James J. Feng, and Savvas G. Hatzikiriakos
Dept. of Chemical and Biological Engineering, The University of British Columbia,
Vancouver, BC, V6T 1Z3, Canada

An approximate mathematical model for polytetrafluoroethylene (PTFE) paste extrusion through annular dies is developed. The model takes into account the elastic–plastic and viscous nature of the material in its nonmelt state arising from the formation of fibrils and the presence of lubricant. The radial flow hypothesis has been used to describe the flow kinematics of PTFE paste in the conical annular section of the die. The validity of this hypothesis is demonstrated by performing numerical simulations using a model recently developed for PTFE paste extrusion. Model predictions are presented for various cases and are found to be consistent with experimental results of macroscopic pressure drop measurements in rod and tube extrusion. © 2006 American Institute of Chemical Engineers *AIChE J,* 52: 4028–4038, 2006
Keywords: PTFE, fibrillation, paste flow, tube extrusion, rod extrusion, radial flow hypothesis

Introduction

Because of its high melting point, polytetrafluoroethylene (PTFE) is processed by techniques such as paste extrusion, cold pressing, and sintering.[1,2] In PTFE paste extrusion, a fine powder of individual particles (diameter $\approx$ 0.25 μm) is first mixed with a lubricating liquid (lube) to form a paste. The paste is then compacted at a typical pressure of 2 MPa to produce a cylindrical tube (preform) that is free of air voids. The next step involves the extrusion of the preform using a ram extruder at a temperature slightly above 30°C where PTFE particles become reasonably deformable.[2] This is usually followed by evaporation of the lubricant by passing the extrudate through an oven. Sintering at high temperatures (380°C) is necessary when full strength is required and porosity must be eliminated for processes such as wire coating and tube fabrication.[2,3]

The flow mechanism associated with PTFE paste extrusion differs significantly from that of polymer melt flow. In paste extrusion, microscopically, PTFE molecules are confined in their crystallite and spherulite configurations, whereas in polymer melt, molecules are randomly positioned, not constricted to a specific shape, and thus are significantly more mobile. Moreover, during paste flow particles mechanically interlock and crystallites unwind to form fibrils that interconnect individual particles.[4] The formation of fibrils provides the good dimensional stability of the final extrudates compared to that of the preforms.[1–4]

Numerous constitutive models have been developed for flows of viscoelastic materials, such as polymer melts,[5] solids under plastic deformations,[6] and elastic–plastic materials that exhibit strain hardening as in the case of metal forming or wire drawing.[7] Although PTFE paste exhibits strain-hardening effects,[1,2,4] little work has been devoted to its flow modeling as an elasto-visco-plastic material.[4] Even with the available equations, significant modifications may still be necessary to improve the model predictions. The empirical equation suggested by Benbow and Bridgwater[3] cannot predict the effect of die entrance angle on the extrusion pres-

Correspondence concerning this article should be addressed to S. G. Hatzikiriakos. at hatzikir@interchange.ubc.ca.

sure of PTFE paste, although it works quite well for other pasty materials.[8,9] Because of its empirical nature, modifications of any theoretical significance are also difficult to incorporate. Also the lubrication approximation used by Benbow and Bridgwater[3] is valid for only a very small entrance angle, which is not consistent with experimental data of PTFE paste extrusion for higher die entrance angle used in rod extrusion.[4,11] An improved analytical model for orifice extrusion of viscoplastic materials was recently proposed.[12] Because of structure formation (fibrillation), strain-hardening effects are obtained at high contraction angles during PTFE flow and therefore these models[3,12] are not suitable for PTFE paste flow through cylindrical and annular dies.

The flow equation suggested by Snelling and Lontz[13] ably and more accurately describes the effects of die design and extrusion speed, although it does not take into account the frictional force, which becomes more important when tapered dies of small entrance angle are used. Also, the analysis provided by Snelling and Lontz[13] does not account for the pressure drop along the capillary length of the die that follows the entrance (contraction) region. Ariawan et al.[4] proposed a viscoplastic model to predict the dependency of extrusion pressure on die geometrical parameters for rod extrusion. This approximate model successfully captured the nonmonotonic dependency of extrusion pressure on die entrance angle and other geometrical characteristics of the cylindrical die. Its derivation is based on the radial flow hypothesis (RFH, discussed below in detail), whose validity was previously demonstrated experimentally.[4,13] Although this model does not explicitly predict micromechanical details of the extrudates, it predicts the extrusion pressure very well and therefore is very useful in die design.[4] On the other hand, tube extrusion (annular flow) is an important process from an industrial perspective, which has not been modeled in the past.

Therefore the main objective of the present work is to generalize the model of Ariawan et al.[4] to tube extrusion and to validate it using numerical simulations and experimental data. As will be evident later, the new model is capable of predicting the processing behavior of paste flow during tube extrusion, such as the extrusion pressure as a function of shear rate and the geometrical characteristics of the die.

The organization of this article is as follows. First, the validity of the RFH is examined by performing flow simulations based on the rheological constitutive model proposed by Patil et al.[14] Then a mathematical model is derived for the case of the annular die based on the developments of Snelling and Lontz[13] and Ariawan et al.[4] Because the model involves the same material parameters as those of the model proposed by Ariawan et al.,[4] these are determined from experimentally measured extrusion pressure for rod extrusion. Model predictions of the dependency of extrusion pressure on the geometrical characteristics of the die agree well with experimental data. Finally, a short summary of the results concludes the article.

Validation of Radial Flow Hypothesis

This hypothesis assumes that the flow is along the radial direction in the die (assuming a spherical system of coordinates as in Figure 1a) and points located on virtual spherical surfaces of a constant radius r from the die apex (Figure 1) have the same radial velocity.[4,13] The mathematical form of the RFH[13] for a cylindrical die (Figure 1a) can be written as

$$\frac{dr}{dt} = -\frac{Q}{2\pi(1 - \cos\alpha)r^2} \quad (1)$$

where Q is the volumetric flow rate and r is the distance from the die apex. Based on this hypothesis, the kinematics of PTFE flow can be calculated at a given volumetric flow rate. Snelling and Lontz[13] and Ariawan et al.[4] experimentally found that the pattern of deformation can be adequately described by the RFH in the conical zone of a tapered cylindrical die (Figure 1a); there is no scientific reason to believe that this would not be true for an annular die. Significant slippage exists in the tapered zone of the die (including in annular dies) and this contributes toward the validity of the RFH.

We examine the validity of the RFH numerically by using the flow model recently developed by Patil et al.[14] These authors proposed a rheological constitutive equation for PTFE paste that takes into account the continuous change of the microstructure during flow through fibril formation. It consists of shear-thinning and shear-thickening terms with their relative contributions to the stress determined by a structural parameter ξ:

$$\boldsymbol{\tau} = (1 - \xi)\boldsymbol{\eta}_1\dot{\gamma} + \xi\boldsymbol{\eta}_2\dot{\gamma} \quad (2)$$

The structural parameter ξ represents the fraction of the domains of the paste that are fibrillated and takes values of 0 and 1 for the unfibrillated and fully fibrillated cases, respectively; $\dot{\gamma}$ is the rate of strain tensor; and η_1 and η_2 are the shear-thinning and shear-thickening viscosities that are expressed by a Carreau model[14]:

$$\eta_i = \eta_{0i}\left[1 + (\lambda_i II_{\dot{\gamma}})^2\right]^{(n_i-1)/2} \quad (3)$$

where $i = 1$ refers to shear-thinning ($n_1 < 1$) and $i = 2$ refers to shear-thickening ($n_2 > 1$). The values of parameters η_{0i}, η_i, and λ_i are the infinite shear viscosity, the zero shear viscosity, and a characteristic relaxation time, respectively.

The evolution of the structural parameter is described by a first-order kinetic differential equation:

$$\mathbf{v} \cdot \nabla\xi = f - g \quad (4)$$

where f and g denote, respectively, the rate of creation and breakage of fibrillated domains in the paste. These functions are given by

$$\left.\begin{array}{l} f(\dot{\gamma}, \psi) = \alpha\dot{\gamma}\sqrt{\psi} \\ g(\dot{\gamma}, \xi) = \beta\dot{\gamma}\xi \end{array}\right\} \quad (5)$$

where α and β are dimensionless rate constants for fibril creation and breakage, both assumed to be 1 in our simulations; Ψ is the flow-type parameter; and $\dot{\gamma}$ is the magnitude of the strain rate tensor. The flow-type parameter Ψ indicates the relative strength of straining and rotation in a mixed flow.[15–17] In the present work, we use finite-element simulations based on this constitutive model to validate the RFH inside the conical section of the die during rod extrusion and tube extrusion
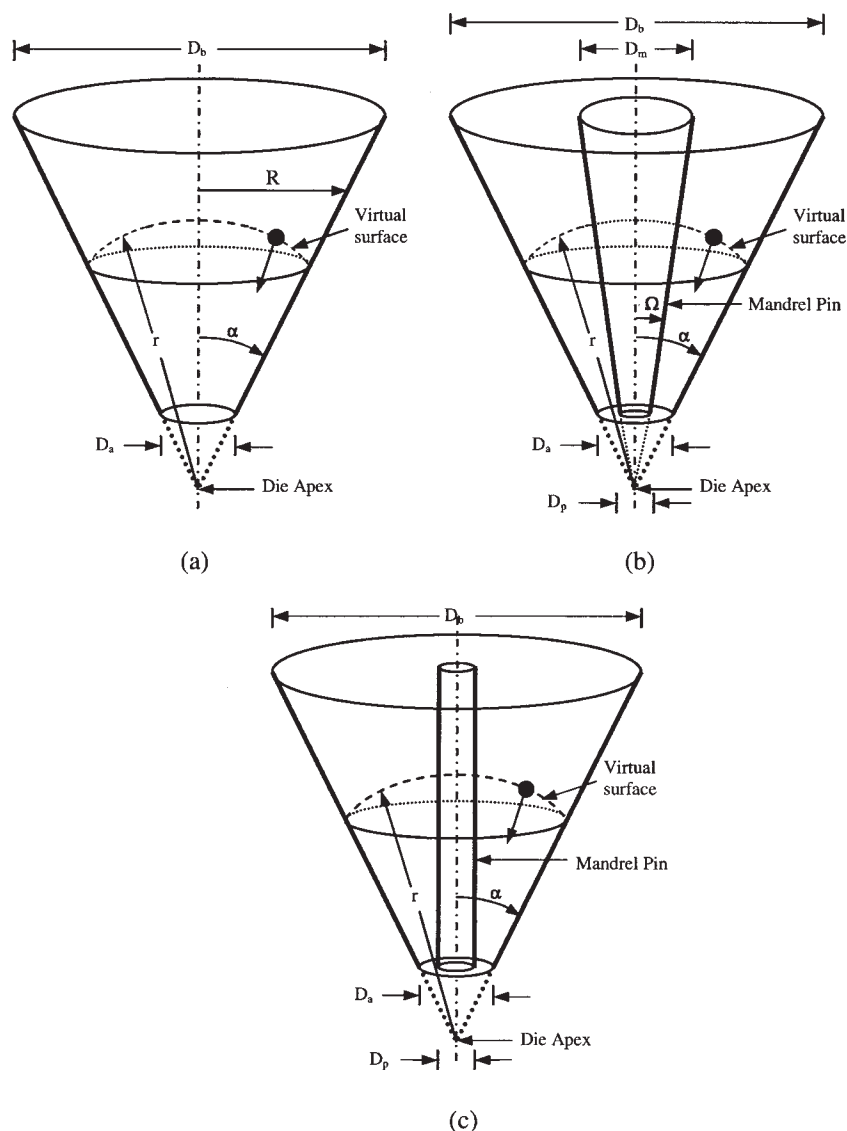
Figure 1. Illustration of the "radial flow" hypothesis.

The hypothesis assumes the existence of a virtual surface of radius r as measured from the die apex, on which all paste particles moving toward the apex have the same velocity: (a) cylindrical die for rod extrusion and (b) annular die with inside cylinder of varying diameter (mandrel pin) for tube extrusion, and (c) annular die with inside cylinder of constant diameter (mandrel pin) for tube extrusion.

(Figure 1). Patil et al.[14] showed that predictions of this model agree very well with macroscopic experimental data of extrusion pressure as a function of flow rate (shear rate) and geometrical characteristics of the die.

Because of the presence of lubricant in the paste, significant slippage occurs at the die walls. This was determined experimentally[14] by establishing a relationship between the slip velocity v_S and the wall shear stress σ_w using the Mooney analysis, $v_S = C\sigma_w$.[18] The simulations in the present study are performed by using the parameters for a paste studied by Ochoa and Hatzikiriakos[19] and Patil et al.,[14] with $C = 1.92$ m·MPa^{-1}·s^{-1}. All the other model parameters are listed in Table 1. Simulations are performed for three different cases sketched in Figure 1: (a) cylindrical die, (b) annular die with an axisymmetric inside cylinder of varying diameter that has the same apex as the outside cylindrical surface, and (c) annular die with an inside cylinder of constant diameter. The geom-

etry in Figure 1b is convenient for mathematical development, but that in Figure 1c is more common in applications.

Cylindrical dies

The simulations are first performed for cylindrical dies with entrance angles of 8, 30, 60, and 90° for various values of the apparent shear rate, defined as $\dot{\gamma}A \equiv 32Q/(\pi D_a^3)$, where Q is the volumetric flow rate and D_a is the capillary diameter at the exit. The inlet and outlet diameters of the

Table 1. Parameters of Eq. 3 Used in the Flow Simulations

Parameter	Shear-thinning	Shear-thickening
η_0 (Pa·s)	4000	1600
λ (s^{-1})	0.3	1
n	0.5	1.3

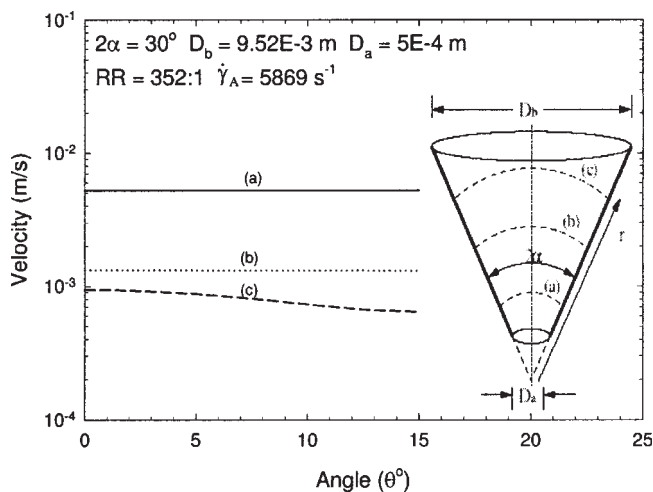**Figure 2. Velocity profiles along the spherical surfaces at radius $r = 5.8 \times 10^{-3}$ m (a), 1.16×10^{-2} m (b), and 1.54×10^{-2} m (c) for cylindrical die ($\theta = 0$ corresponds to the centerline).**

conical section are $D_b = 9.52 \times 10^{-3}$ m and $D_a = 5.08 \times 10^{-4}$ m, respectively. These are typical die dimensions used in experiments that are presented later. To demonstrate the validity of the RFH, radial velocity profiles are plotted vs. angle θ ($-\alpha \leq \theta \leq \alpha$) along the virtual peripheral surfaces at constant radial positions from the die apex. Figure 2 shows representative velocity profiles at three different radial positions from the die apex for a die entrance angle of 30°. This indicates that the velocity variation from the centerline to die wall is generally small and in agreement with the RFH, which implies flat velocity profiles. A small variation in the velocity profile occurs at the inlet to the die, which is considered unimportant because the contribution of this part of the flow to the overall pressure drop is negligible.

Figure 3 depicts the percentage variation of velocity, defined as the difference between velocity at the centerline and the die wall normalized by the centerline velocity, plotted against the die entrance angle at three radial locations (a), (b), and (c). The radial positions (a), (b), and (c) are given by $r = R/\sin \alpha$, where R and α indicate corresponding cylindrical radius and die entrance angle (Figure 1a). In Figures 3, 5, and 7 the three cylindrical locations $R = 1.5 \times 10^{-3}$, 3.0×10^{-3}, and 4.0×10^{-3} m are identical, although corresponding radial locations (a), (b), and (c) vary with die entrance angle. The variation of the velocity profile is significant only for (c) near the inlet for dies of high entrance angle. This variation decreases rapidly in the downstream direction and, in fact, in the middle of the die [location (b)] becomes insignificant. At position (b), the velocity variation is 12% for dies having an entrance angle of 90° and 2.1% for dies having an entrance angle of 60°. For die entrance angles $2\alpha \leq 60°$ (typically used in paste extrusion) the variation is negligible and therefore the RFH applies.

To study the effect of the apparent shear rate $\dot{\gamma}_A$ and the die reduction ratio $RR \equiv D_b^2/D_a^2$ on the velocity variation along the virtual peripheral surfaces at constant r from the die apex, simulations are performed for a cylindrical die having an entrance angle of $2\alpha = 30°$ and a reduction ratio $RR = 352$, for

apparent shear rate values ranging from 1875 to 8304 s^{-1}. Near the outlet [position (a)], the percentage velocity variation normalized by the centerline velocity is found to be 0.015 and 0.026% for the apparent shear rates of $\dot{\gamma}_A = 1875$ s^{-1} and $\dot{\gamma}_A = 8304$ s^{-1}, respectively. Similarly at position (b), the normalized velocity variations are 0.23 and 0.33% for the apparent shear rates of $\dot{\gamma}_A = 1875$ s^{-1} and $\dot{\gamma}_A = 8304$ s^{-1}, respectively. Simulations were also performed for various die reduction ratios ranging from 56 to 567 at the apparent shear rate of 5869 s^{-1}. The percentage velocity variations are 0.058 and 0.02% at position (a) for $RR = 56$ and 567, respectively. At position (b), they are 0.8 and 0.24%. Therefore, the RFH is more accurate at lower flow rates and large reduction ratios.

Annular die with varying diameter mandrel pin

Simulations were also performed for annular dies with an axisymmetric inside surface of varying diameter (mandrel pin) having the same apex with the outside cylindrical surface (Figure 1b). The existence of a single apex produces a die geometry that allows the development of an analytical flow model (see Mathematical Model section below) in spherical coordinates (r and θ define the entire flow field). Simulations were performed for various die entrance angles ranging from 8 to 90° at various values of apparent shear rate $\dot{\gamma}_A$, which is defined as $\dot{\gamma}_A \equiv 48Q/\pi(D_a - D_p)^2(D_a + D_p)$, where Q is the volumetric flow rate. The die and mandrel diameters at the inlet are $D_b = 9.5 \times 10^{-3}$ m and $D_m = 3.0 \times 10^{-3}$ m, respectively, and at the outlet are $D_a = 5.08 \times 10^{-4}$ m and $D_p = 1.6 \times 10^{-4}$ m, respectively (Figure 1b). The coincidence of the apex requires $D_p = D_m(D_a/D_b)$. Figure 4 depicts representative velocity profiles along the virtual peripheral surfaces at three various radial positions from the die apex for a die entrance angle of 30° (see inset of Figure 4). These are qualitatively similar to the profiles in the cylindrical dies (Figure 2). Small variations in the velocity profiles are obtained only at the inlet (c) and their contributions to the overall pressure drop are insignificant.

Figure 5 shows the percentage variation of velocity normalized by the velocity on the mandrel surface, plotted against the
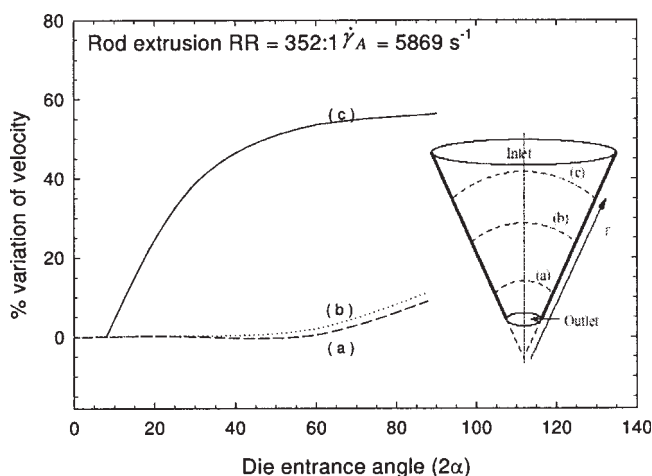

Figure 3. Percentage variation of velocity normalized by the centerline velocity, from the centerline to the die wall plotted with die entrance angle.

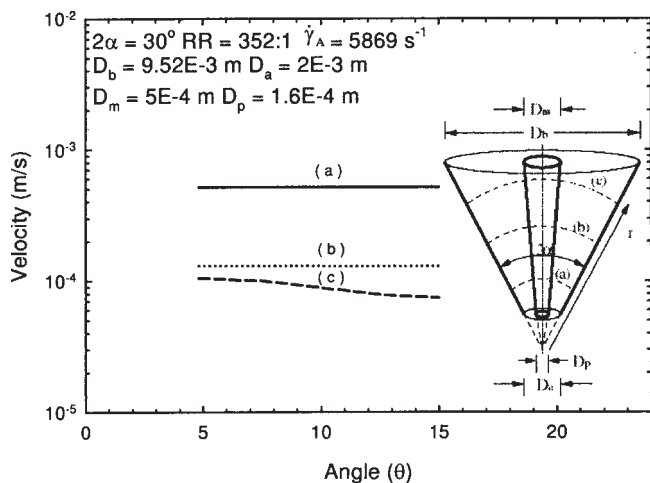The three surfaces are defined by the cylindrical radius $R = 1.8 \times 10^{-3}$ m (a), 3.0×10^{-3} m (b), and 4.0×10^{-3} m (c).

Figure 4. Velocity profiles along the spherical surfaces at radius $r = 5.8 \times 10^{-3}$ m (a), 1.6×10^{-2} m (b), and 1.54×10^{-2} m (c) for an annular die with inside cylinder of varying diameter.

$\theta = 15°$ corresponds to the outside wall; $\theta = 0°$ does not exist because of the presence of the internal mandrel pin.

die entrance angle at the same radial locations. The variation of velocity is significant only near the inlet [location (c)] and increases with die entrance angle. However, variations in velocity over the lower portion of the die that contribute significantly to the pressure drop are very small for dies having die entrance angles up to 60° (typically used in extrusion operation). Therefore the RFH can be used safely for dies up to entrance angles of 60°.

Annular die with axisymmetric cylindrical mandrel pin

Similar simulations were performed for annular dies with an inside cylinder of constant diameter (mandrel pin) as depicted in Figure 1c. The die entrance angle ranges from 8
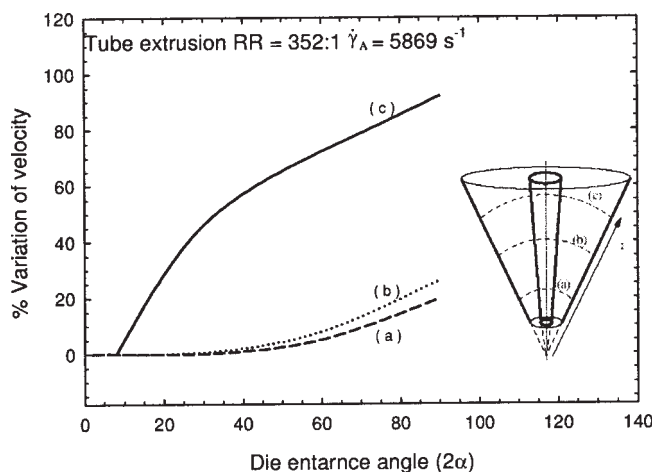

Figure 5. Percentage variation of velocity from the wall of the varying diameter mandrel pin to the die wall normalized by the velocity at the wall of the varying diameter cylinder, plotted with die entrance angle at three different spherical locations (a), (b), and (c) defined in Figure 3.
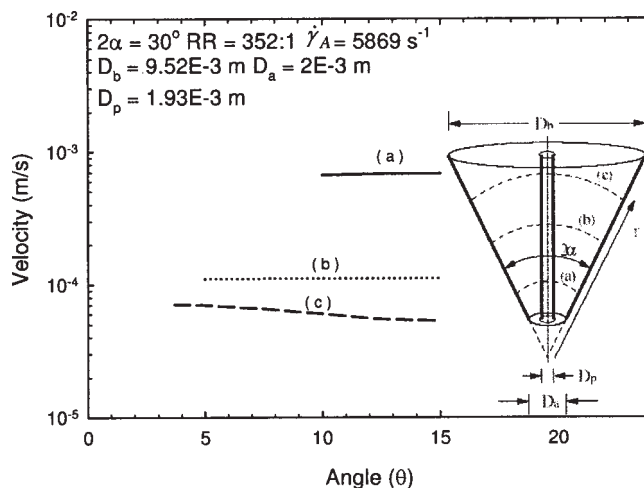

Figure 6. Velocity profiles along the spherical surfaces at radius $r = 5.8 \times 10^{-3}$ m (a), 1.6×10^{-2} m (b), and 1.54×10^{-2} m (c) for an annular die having a mandrel pin of constant diameter.

to 90°. The outer diameter of inlet of the conical section of the die is $D_b = 9.5 \times 10^{-3}$ m, the outer diameter of outlet is $D_a = 2.0 \times 10^{-3}$ m, and the diameter of the axisymmetric constant diameter cylinder is $D_p = 1.9 \times 10^{-3}$ m (Figure 1c). Although the analytical mathematical model will be derived for an annular die having a single apex (Figure 1b), it can still be used for annular dies with cylindrical mandrel pins, once the RFH is proven for this geometry.

Figure 6 depicts representative velocity profiles along the virtual peripheral surfaces at three radial positions from the die apex for a die having an entrance angle of 30° (see inset of Figure 6). The results are similar to those discussed earlier. Small variations in the velocity profiles are obtained only at the inlet to the die. Figure 7 shows the percentage variation of velocity normalized by the centerline velocity on the mandrel surface, plotted against the die entrance angle at the three radial locations. The variation of velocity is significant only near the inlet and only for dies having a large entrance angle. The variation in velocity profile over most of the die is very small and increases up to 14.8% for a die entrance angle of 90°. This clearly indicates that the "radial flow" hypothesis can be used safely for annular dies having an entrance angle of up to 60°. In a comparison of Figures 5 and 7, it will seem to the observer that the RFH applies better in annular dies having mandrel pin of constant diameter.

Mathematical Model

Now that the validity of RFH has been established for cylindrical and annular dies, an analytical model will be derived to describe annular flow of PTFE paste. It is based on the RFH and generalizes the earlier model of Ariawan et al.[4] for annular dies.

Annular die without die land ($L/D_a = 0$)

Consider first an annular die without the cylindrical die land (Figure 1b). Figure 8b shows a volume element bounded
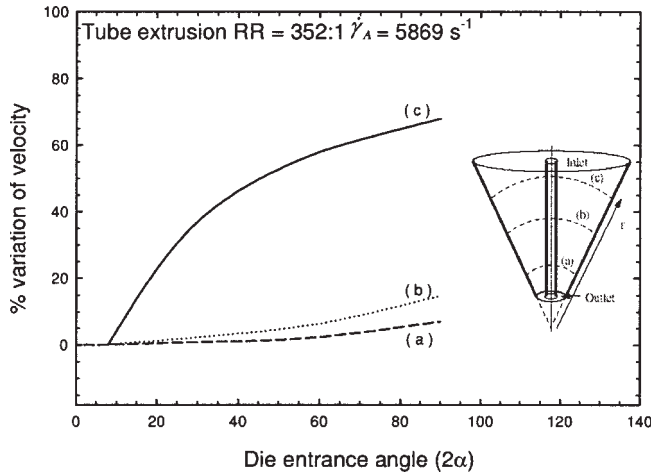
Figure 7. Percentage variation of velocity from the wall of the constant diameter mandrel pin to the die wall normalized by the velocity at the wall of the constant diameter cylinder, plotted with die entrance angle at three different spherical locations (a), (b), and (c) defined in Figure 3.

by the spherical surfaces of radius r and $(r + dr)$ as measured from the virtual die apex, and by four planes at the azimuthal locations of θ, $\theta + d\theta$, ϕ, and $\phi + d\phi$. The RFH implies that this element will flow toward the die apex, such that its bounding surfaces remain parallel to those at its previous position. Because the element does not rotate or deviate from its straight path, this also implies that the stresses acting on the element are purely normal stresses. In fact, these stresses are principal stresses, with the radial direction and the directions normal to the four bounding planes as the principal directions:

$$\sigma = \begin{bmatrix} \sigma_{\mathrm{I}} & 0 & 0 \\ 0 & \sigma_{\mathrm{II}} & 0 \\ 0 & 0 & \sigma_{\mathrm{III}} \end{bmatrix} = \begin{bmatrix} \sigma_r & 0 & 0 \\ 0 & \sigma_\theta & 0 \\ 0 & 0 & \sigma_\phi \end{bmatrix} \quad (6)$$

We further assume $\sigma_\theta = \sigma_\phi$ to simplify the mathematics. In reality, the squeezing in the θ and ϕ directions is comparable in magnitude if not equal. The force balance on the volume element (see Figure 8b) in the radial direction gives rise to an equilibrium relation:

$$-2\pi r^2(\cos\Omega - \cos\alpha)d\sigma_r - 4\pi r(\cos\Omega - \cos\alpha)\sigma_r \, dr$$
$$+4\pi\sigma_\theta r(\cos\Omega - \cos\alpha)dr + 2\pi f\sigma_\theta r(\sin\Omega + \sin\alpha)dr = 0 \quad (7)$$

where $\Omega = \tan^{-1}[(D_m/D_b)\tan\alpha]$ and f is the coefficient of friction. By letting $B = f(\sin\Omega + \sin\alpha)/2(\cos\Omega - \cos\alpha)$ and $N_1 = \sigma_r - \sigma_\theta$, and rearranging, we obtain

$$\frac{d\sigma_r}{dr} - 2B\frac{\sigma_r}{r} = \frac{2(\sigma_\theta - \sigma_r)(1+B)}{r} = \frac{-2N_1(1+B)}{r} \quad (8)$$

The term N_1 is similar to the first normal stress difference in polymer rheology, except that, in this case, it is for a

nonviscometric flow. To solve the above differential equation, a relationship describing the first normal stress difference for the solid–liquid (paste) system in question is thus required. For an ideally plastic material, Saint-Venant's theory of plastic flow gives $N_1 = \sigma_0$ at the incipience of yielding, where σ_0 is the initial yield stress of the material.[20] However, for a completely plastic flow to occur within an elasto-visco-plastic material, N_1 has to sufficiently exceed σ_0 so as to overcome the initial yield stress, the elastic stress, and any viscous resistance that may develop during the flow.[6,21]

The generalized Newton's law for viscous flow states that $\boldsymbol{\sigma} = \eta\dot{\boldsymbol{\varepsilon}}$ and Hooke's law of elasticity establishes the relationship $\boldsymbol{\sigma} = E\boldsymbol{\varepsilon}$, where η and E are the viscosity coefficient and the Young's modulus, respectively, and ε and $\dot{\varepsilon}$ are the logarithmic strain and strain rate tensors, respectively. Combining the two laws gives the following stress–strain relationship for a viscoelastic material[6]:

$$\boldsymbol{\sigma} = E\boldsymbol{\varepsilon} + \eta\dot{\boldsymbol{\varepsilon}} \quad (9)$$

Using the above relation, the term $\sigma_\theta - \sigma_r$ adopts the form of

$$\sigma_\theta - \sigma_r = E(\varepsilon_\theta - \varepsilon_r) + \eta(\dot{\varepsilon}_\theta - \dot{\varepsilon}_r) \quad (10)$$

where $\varepsilon_\theta - \varepsilon_r = \varepsilon_{\mathrm{II}} - \varepsilon_{\mathrm{I}}$ and $\dot{\varepsilon}_\theta - \dot{\varepsilon}_r = \dot{\varepsilon}_{\mathrm{II}} - \dot{\varepsilon}_{\mathrm{I}}$ are the maximum strain γ_{max} and the maximum strain rate $\dot{\gamma}_{\mathrm{max}}$, respectively. The term "maximum strain" was introduced by Ludwik,[22] who realized that N_1 should be a unique function of γ_{max}. Ludwik is also credited with the modified Hooke's law expression that takes the final form of a power law equation

$$\boldsymbol{\sigma} = C\boldsymbol{\varepsilon}^n \quad (11)$$

where C is Young's modulus when $n = 1$.

Because of the presence of both the liquid and solid phases in the PTFE paste system, it is necessary to consider PTFE paste as an elasto-visco-plastic material. To model its flow, the expression suggested by Snelling and Lontz[13] is adopted, which is essentially the Kelvin stress–strain relation Eq. 9, with modifications that are similarly used in the Ludwik power law model Eq. 11 for the elastic (strain-hardening) term, and the generalized power law model for the viscous resistance term. The resulting expression for the first normal stress difference N_1 is then written as follows:

$$\sigma_\theta - \sigma_r = C\gamma_{\mathrm{max}}^n + \eta\dot{\gamma}_{\mathrm{max}}^m \quad (12)$$

A more general three-dimensional form of Eq. 12 can be written by considering the general model for an elastic solid, such as that used by Rivlin,[23,24] and for a viscous fluid, in terms of the invariant functions of the strain and strain rate tensors, respectively.[25] However, the objective here is to derive a simple analytical flow model to be compared with macroscopic extrusion pressure measurements.

To account for the initial yield stress, an additional term may be included on the right-hand side of Eq. 12. However, this term is expected to be negligible compared to the other terms, as indicated by the fact that the initial strength of the preform is much weaker than that of the extrudate.
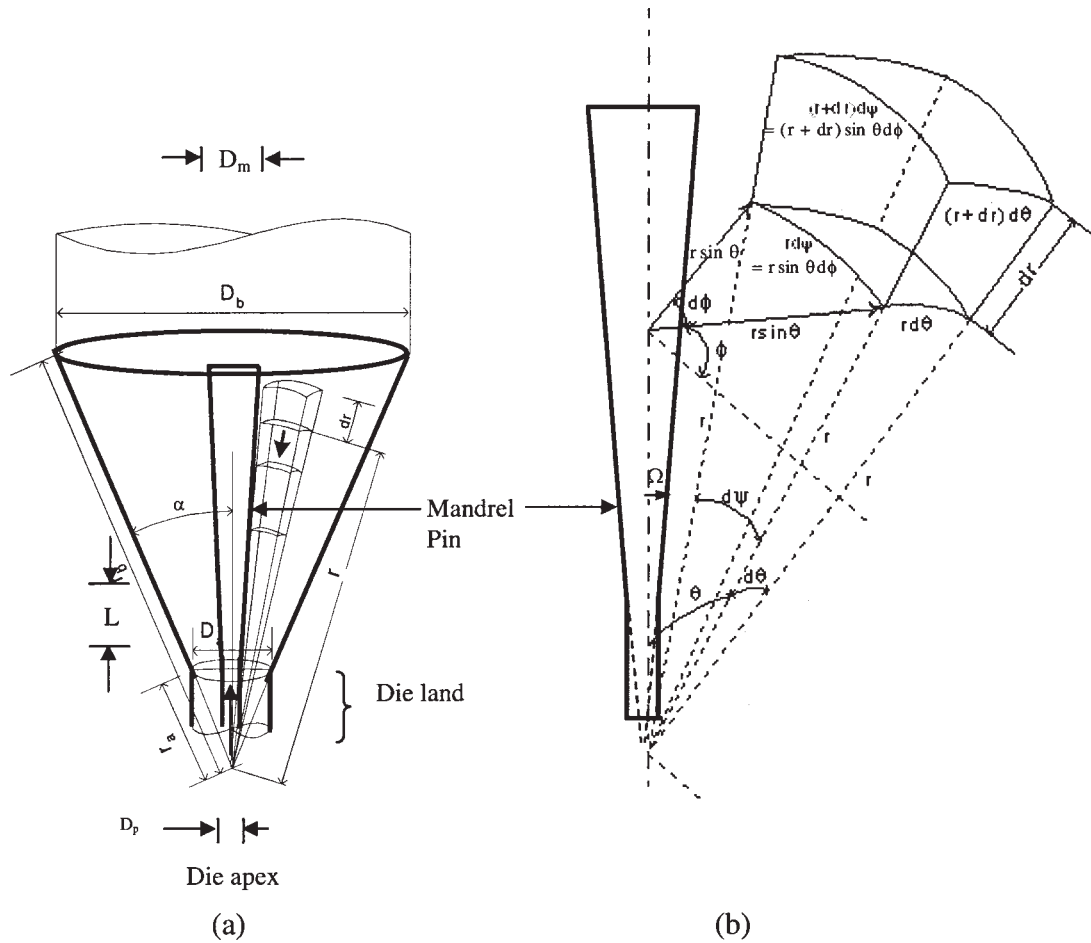
Figure 8. (a) Annular die with varying diameter mandrel pin with volume element and (b) its dimensions in the annular conical zone of a tapered die according to "radial flow" hypothesis.

Now, it can be shown that the volume element at a distance r_b from the virtual die apex experiences a maximum strain of

$$\gamma_{max} = \varepsilon_\theta - \varepsilon_r = 3\varepsilon_\theta$$
$$= 3\int_{r_b}^r \frac{dr}{r} = -3\ln\frac{r_b}{r} \qquad (13)$$

The maximum strain rate can then be expressed as

$$\dot{\gamma}_{max} = \frac{d\gamma_{max}}{dt} = 3\frac{dr}{rdt} \qquad (14)$$

The "radial flow" hypothesis for annular conical dies of single apex can be written as

$$\frac{dr}{dt} = -\frac{\text{Volumetric flow rate}}{\text{Area of surface}} = -\frac{Q}{2\pi(\cos\Omega - \cos\alpha)r^2} \qquad (15)$$

Thus, the maximum strain rate is (see Eq. 14)

$$\dot{\gamma}_{max} = \frac{3Q}{2\pi(\cos\Omega - \cos\alpha)r^3} \qquad (16)$$

and the normal stress difference is

$$N_1 = \sigma_r - \sigma_\theta = C\left[3\ln\left(\frac{r_b}{r}\right)\right]^n + \eta\left[\frac{3Q}{2\pi(\cos\Omega - \cos\alpha)r^3}\right]^m \qquad (17)$$

Substituting the above into Eq. 8 yields the following expression:

$$-\sigma_r = 2(1+B)r^{2B}\left\{C\int\frac{[3\ln(r_b/r)]^n}{r^{2B+1}}dr \right.$$
$$\left. + \frac{\eta}{-(3m+2B)}\left[\frac{3Q}{2\pi(\cos\Omega - \cos\alpha)}\right]^m\left(\frac{1}{r^{3m+2B}}\right)\right\} + r^{2B}\hat{C} \qquad (18)$$

where the constant of integration $\hat{C}$ is evaluated using the boundary condition $\sigma_r = \sigma_{ra}$ when $r = r_a$:

$$\hat{C} = -\frac{\sigma_{ra}}{r_a^{2B}} - 2(1+B)\left\{C\int_{r_a}\frac{[3\ln(r_b/r)]^n}{r^{2B+1}}dr \right.$$
$$\left. + \frac{\eta}{-(3m+2B)}\left[\frac{3Q}{2\pi(\cos\Omega - \cos\alpha)}\right]^m\left(\frac{1}{r_a^{3m}+2B}\right)\right\} \qquad (19)$$

The extrusion pressure can then be calculated using Eqs. 8 and 12 with $r = r_b$, that is,

$$P_{extrusion} = \sigma_{rb} = \sigma_{ra}RR^B + 2(1+B)$$
$$\times\left\{C\left(\frac{D_b}{2\sin\alpha}\right)^{2B}\int_{r_a=D_a/2\sin\alpha}^{r_b=D_b/2\sin\alpha}\frac{[3\ln(r_b/r)]^n}{r^{2B+1}}dr + \frac{\eta}{(3m+2B)}\right.$$
$$\left. \times\left[\frac{12Q\sin^3\alpha}{\pi(\cos\Omega - \cos\alpha)D_b^3}\right]^m\left[RR^{B+(3m/2)} - 1\right]\right\} \qquad (20)$$

where σ_{ra} is the stress at the die exit; RR is the reduction ratio of larger to smaller cross-sectional area of annular conical section inlet and outlet, respectively, defined as $(D_b^2 - D_m^2)/(D_a^2 - D_p^2)$; and C, η, n, m, and f are material constants that have to be determined experimentally.

When an orifice die is used, σ_{ra} may be present at the die exit as the result of a pulling force during extrudate wind-up or calendering. However, σ_{ra} is typically negligible and the expression for extrusion pressure can then be simplified to

$$P_{extrusion} = 2(1+B)\left\{ C\left(\frac{D_b}{2\sin\alpha}\right)^{2B} \int_{r_a = D_a/2\sin\alpha}^{r_b = D_b/2\sin\alpha} \frac{[3\ln(r_b/r)]^n}{r^{2B+1}} dr \right.$$
$$\left. + \frac{\eta}{(3m+2B)}\left[\frac{12Q\sin^3\alpha}{\pi(\cos\Omega - \cos\alpha)D_b^3}\right]^m \left[RR^{B+(3m/2)} - 1\right] \right\} \quad (21)$$

Numerical integration is required in Eq. 21. However, for a range of the die reduction ratio of interest, the following approximation can be used with reasonable accuracy in Eq. 21, allowing an analytical solution to be obtained:

$$\ln(r_b/r) \approx a(r_b/r)^b \quad (22)$$

where a and b are constant fitting parameters.

Annular die with die land ($L/D_a \neq 0$)

Additional pressure drop in the die land can be computed using a similar force balance. The forces acting on a volume element in the capillary zone are shown in Figure 9. A force balance on the element yields

$$(\sigma_z + d\sigma_z)\pi\frac{D_a^2 - D_p^2}{4} - \sigma_z\pi\frac{D_a^2 - D_p^2}{4} = f\sigma_{r'}\pi(D_a + D_p)dz \quad (23)$$

or

$$\frac{d\sigma_z}{dz} = \frac{4f\sigma_{r'}(D_a + D_p)}{(D_a^2 - D_p^2)} = \frac{4(D_a + D_p)f(N_1 + \sigma_z)}{(D_a^2 - D_p^2)} \quad (24)$$

where N_1 is the previously defined first normal stress difference, which is expected to be significant as a result of the elastic nature of PTFE paste. At the end of the die conical zone (thus, at the entrance of the die capillary zone), N_1 can be calculated using Eq. 17 with $r = r_a$. Assuming N_1 to be approximately constant throughout the capillary zone of the die, the force balance becomes

$$\frac{d\sigma_z}{dz} = \frac{4(D_a + D_p)f(N_{1a} + \sigma_z)}{(D_a^2 - D_p^2)} \quad (25)$$

where

$$-N_{1a} = C\left[\frac{3}{2}\ln(R)\right]^n + \eta\left[\frac{12Q\sin^3\alpha R^{3/2}}{\pi(\cos\Omega - \cos\alpha)D_b^3}\right]^m$$

Solving Eq. 24 and applying the boundary condition $\sigma_z = \sigma_{zL}$ at $z = L$, yields

$$\sigma_z = N_{1a}\left[e^{4f(z-L)(D_a+D_p)/(D_a^2-D_p^2)} - 1\right]$$
$$+ \sigma_{zL}e^{4f(z-L)(D_a+D_p)/(D_a^2-D_p^2)} \quad (26)$$

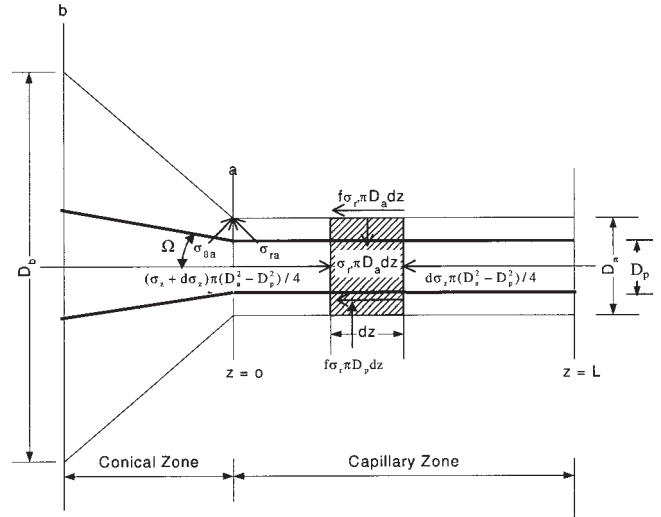where σ_{zL} is the stress imposed at the exit of the die, which is typically negligible or zero.

Figure 9. Force balance on volume element in the die capillary zone.

The stress present at the entrance of the die capillary zone (σ_{z0}) is obtained from Eq. 26 with $z = 0$:

$$\sigma_{z0} = N_{1a}\left[e^{-4f(D_a+D_p)L/(D_a^2-D_p^2)} - 1\right] + \sigma_{zL}e^{-4f(D_a+D_p)L/(D_a^2-D_p^2)} \quad (27)$$

By putting $\varepsilon = (1 - D_p)/D_a$ in Eq. 27, σ_{z0} can be written as

$$\sigma_{z0} = N_{1a}(e^{-4fL/\varepsilon D_a} - 1) + \sigma_{zL}e^{-4fL/\varepsilon D_a} \quad (28)$$

The total extrusion pressure can be obtained by substituting $\sigma_{ra} = -\sigma_{z0}$ into Eq. 20.

Model Predictions and Comparison with Experiments

In this section the dependency of the extrusion pressure on the apparent shear rate, the die entrance angle (2α), and the die reduction ratio (RR) is predicted by using the proposed model (Eq. 20), for cylindrical (Figure 1a) and annular dies (Figure 1b) with no die land section. Extrusion experiments were performed with cylindrical dies using two PTFE fine powder resins supplied by Solvay-Solexis (Milan, Italy) of primary and secondary particle diameters of 0.25 and 450–550 μm, respectively, and standard specific gravity of 2.16. The paste was prepared by mixing resins with isoparaffinic liquid as lubricant (Isopar® H) supplied by ExxonMobil Chemical (Houston, TX) with properties listed in Table 2. The two resins have different molecular weights and are labeled as resins A and B in Table 3. The material parameters C, n, η, m, and f in Eq. 20 are evaluated by fitting a single set of experimental data for resins A and B in a cylindrical die (see Figure 10).[4] Dimensions of the cylindrical die are: $D_b = 9.5 \times 10^{-3}$ m, $D_a = 5.0 \times 10^{-4}$ m, and the die entrance angle was $2\alpha = 60°$. The model parameters C, n, η, m, and f are determined by nonlinear dynamic optimization using a Gauss–Newton iterative algorithm that minimizes the difference between model predictions of the extrusion

Table 2. Physical Properties of Isopar®/ H Lubricant

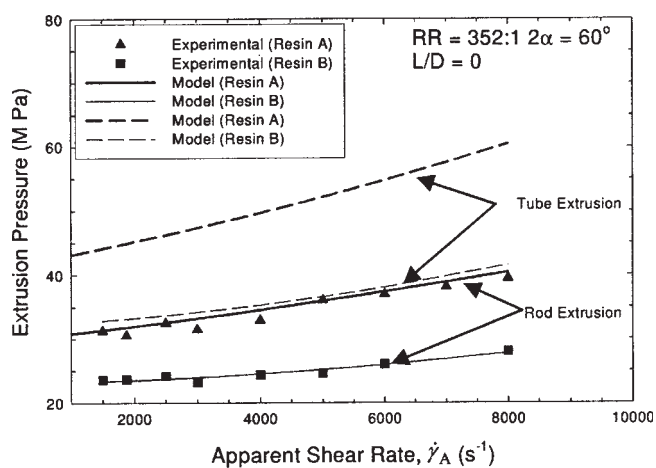| Property	Isopar®/ H
Specific gravity, kg/m³ (25°C)	760
Surface tension, N/m (25°C)	2.37×10^{-2}
Vapour pressure, Pa (38°C)	104
Viscosity, Pa·s (25°C)	1.09×10^{-3}

Figure 10. Effect of apparent shear rate on the extrusion pressure of PTFE paste for a cylindrical (rod extrusion) and an annular conical die (tube extrusion).

The experimental data refer to rod extrusion using an orifice die ($L/D = 0$), having $RR = 352$, $2\alpha = 60°$.

pressure and the measured values. The standard deviations for all these parameters were <5%. The fitted values of the parameters are listed in Table 3 for resins A and B. Because these are material parameters independent of the die geometry, they can be used in predicting extrusion pressure for cylindrical and annular dies of different geometry, as long as the "radial flow" hypothesis is valid. Note the small value of the friction factor f, which implies that the pressure drop in the die land is much smaller compared to that in the conical zone. Typically, the pressure drop in the die land can account for about 5% of the total pressure drop for short dies ($L/D_a = 5$) to 30% for long dies ($L/D_a = 40$), depending on the type of resin.

Figure 10 plots the extrusion pressure for resins A and B in rod extrusion. The solid lines indicate model prediction using parameters determined by best fitting of the experimental data. The steady-state extrusion pressure generally increases with increasing apparent shear rate. Although resin A has a lower viscosity than that of resin B, it has a larger elastic constant, and the strain-hardening effect leads to a higher pressure drop than that of resin B. The dotted lines indicate model predictions for tube extrusion using the same model parameters. As expected, the extrusion pressure for annular dies is higher than that for cylindrical dies under comparable conditions because of the presence of the additional inside cylinder wall.

Once the material parameters are determined, the model can be used to predict the effects of die geometry on extrusion pressure. Figure 11 shows the model predictions for the dependency of extrusion pressure on the die reduction ratio for cylindrical die and annular die with varying diameter mandrel pin (Figure 1b) using the parameters for resin A. The reduction ratio of the die is increased by decreasing the small diameter D_a for the cylindrical die, and both D_a and D_p for the annular die. The nonlinear dependency of extrusion pressure on the die reduction ratio is clearly seen.

Figure 12 depicts the model prediction for the dependency of the extrusion pressure on the die entrance angle for cylindrical and annular dies. One observes that the extrusion pressure initially decreases and goes through a minimum until it again increases with increasing die entrance angle. In both cylindrical and annular dies, the minimum extrusion pressure is required for a die with die entrance angle of around 8°. This value depends on the value of the material parameters.

To further test the validity of the proposed mathematical model, experiments were performed using resin B in an annular die with a cylindrical die land attached. The annular die has an exit diameter of $D_a = 6.48 \times 10^{-3}$ m, a mandrel pin of diameter $D_p = 4.7 \times 10^{-3}$ m, a die entrance angle of $2\alpha = 180°$, a length to diameter ratio $L/D_a = 35$, and a reduction ratio of $(D_b^2 - D_p^2)/(D_a^2 - D_p^2) = 35$. Details for the experimental procedure can be found in previous publications.[4,19,26,27] Figure 13 compares the measured steady-state extrusion pressure as a function of the apparent shear rate with model predictions using the fitted values of the various parameters listed in Table 3. The agreement between the two is excellent and indicates that our model is capable of accurate description of paste extrusion for both cylindrical and annular dies.
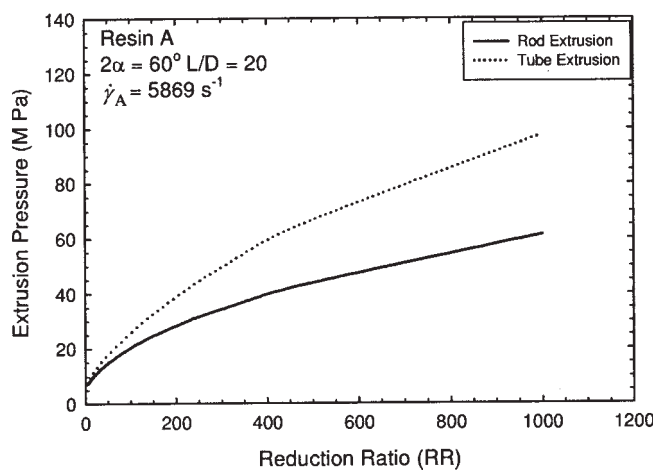

Figure 11. Effect of die reduction ratio on the extrusion pressure of PTFE paste for a cylindrical (rod extrusion) and an annular die (tube extrusion).

Table 3. Values of Material Constants and Coefficient of Friction Needed in Eq. 25 to Predict the Extrusion Pressure for Paste Slow in Cylindrical and Annular Dies

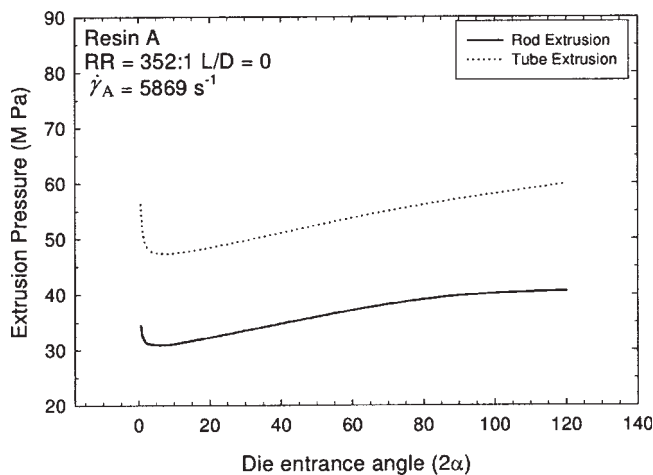| Resin	C (MPa)	n	η (MPa·s)	m	f
A	1.14×10^{-1}	2.28	1.25×10^{-3}	1.21	1.3×10^{-4}
B	8.92×10^{-2}	2.13	3.56×10^{-3}	1.11	1.12×10^{-4}

Figure 12. Effect of die entrance angle (2α) on the extrusion pressure of PTFE paste for a cylindrical die (rod extrusion) and an annular die (tube extrusion).

Conclusions

Numerical simulations were performed for conical and annular dies by using a combined shear-thinning and shear-thickening rheological constitutive model proposed by Patil et al.[14] to study the validity of the RFH during PTFE paste flow. The numerical results have shown that the "radial flow" hypothesis is valid for both cylindrical and annular dies having a contraction angle up to 60°. Based on these findings, a simple flow model is developed to predict the dependency of extrusion pressure on the extrusion speed (apparent shear rate) in annular dies. The model considers the paste as an elasto-visco-plastic material that exhibit both strain-hardening and viscous resistance effects during flow. Comparison with limited experimental data from both cylindrical and annular dies was found to validate the usefulness of this analytical and approximate but simple model. The
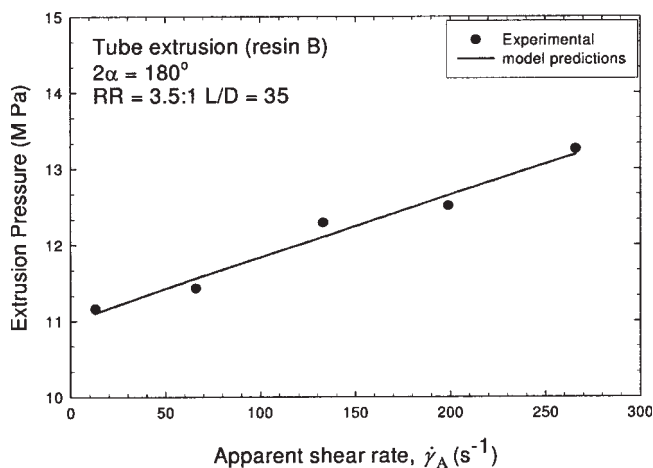
model successfully predicts the dependency of extrusion pressure on apparent shear rate for tube extrusion using model parameters determined by fitting data for rod extrusion. The model was also used to predict the dependency of extrusion pressure on die geometrical parameters.

A final comment relates to the limitations of the model. Although the extrusion pressure can be well predicted as a function of the operating parameters and the geometrical characteristics of the dies, the material's structure (fraction of fibrillated domains) is not explicitly calculated. This limitation is the subject of a future study and it would be ideal to have an analytical model that can relate flow kinematics and structure with the mechanical properties of the final extrudates as in the numerical flow model of Patil et al.[14]

Acknowledgments

Notation

$M_M, M_{MM}, M_{MMM}a$, b = fitting parameters (Eq. 22)

B = model parameter defined as $f(\sin \Omega + \sin \alpha)/2(\cos \Omega - \cos \alpha)$

C = proportionality constant for the elastic term in Eq. 11, Ludwik's power law model

$\hat{C}$ = constant of integration

D_a = die exit diameter

D_b = die entrance diameter

D_m = mandrel diameter at the inlet of the annular die

D_p = mandrel diameter at the exit of the annular die

E = Young's modulus of elasticity

f = Coulomb's law coefficient of friction, between PTFE paste and die wall

f = rate of creation of fibrillated domains (Eq. 5)

g = rate of breakage of fibrillated domains (Eq. 5)

L = length of die land

m = power law index for the viscous term of Eq. 12

n_i, n = power law indices for the elastic term of Eqs. 3 and 12, ($i = 1, 2$)

N_1, N_{1a} = first normal stress difference (N_{1a} is the first normal stress difference calculated at the exit of the die)

$P_{extrusion}$ = extrusion pressure

Q = volumetric flow rate

RFH = "radial flow" hypothesis

RR = die surface reduction (contraction) ratio

R_a = average roughness

r, θ, ϕ = spherical coordinate axes used in force analysis in the die conical (entrance) zone (if used as subscripts, these indicate the directions in which a particular vector is acting)

r_b, r_a = radial distances as measured from the virtual die apex to the entrance and exit of the die conical zone, respectively

t = time

v = velocity field vector

v_S = slip velocity

z = axial coordinate

Greek letters

$M_M, M_{MM}, M_{MMM}\alpha$ = half die entrance angle

α, β = dimensionless rate constants used only in Eq. 5

$\dot{\gamma}$ = rate of strain tensor

Figure 13. Effect of apparent shear rate on the extrusion pressure of PTFE (resin B) paste for an annular die (tube extrusion).

$\dot{\gamma}_A$ = apparent shear rate

$\gamma_{max}, \dot{\gamma}_{max}$ = maximum strain and strain rate, respectively (maximum strain is defined as the difference of strains in the first two principal directions)

$\varepsilon_I, \varepsilon_{II}, \varepsilon_{III}$ = strains in the three principal directions

$\varepsilon_r, \varepsilon_\theta, \varepsilon_\phi$ = strains in the three principal directions

$\varepsilon, \dot{\varepsilon}$ = strain and strain rate, respectively

η = viscosity coefficient

η_0 = zero shear viscosity in Eq. 3

η = infinite shear viscosity in Eq. 3

λ_i = characteristic relaxation times in Eq. 3 ($i = 1, 2$)

ξ = structural parameter that represents the fraction of the fibrillated domains

σ = stress

σ_w = wall shear stress

$\sigma_I, \sigma_{II}, \sigma_{III}$ = stresses in the three principal directions

$\sigma_r, \sigma_\theta, \sigma_\phi$ = stresses in the three principal directions

σ_0 = yield stress

τ = stress tensor

Ψ = flow type parameter

Ω = angle of the mandrel pin

Literature Cited

1. Mazur S. Paste extrusion of poly(tetrafluoroethylene) fine powders. In: Narkis M, Rosenzweig N, eds. *Polymer Powder Technology*. New York: Wiley; 1995:441–482.
2. Ebnesajjad S. *Fluoroplastics: Non-Melt Processible Fluoroplastics*. New York: William Andrew; 2000: Vol. 1.
3. Benbow JJ, Bridgwater J. *Paste Flow and Extrusion*. Oxford, UK: Oxford Univ. Press; 1993.
4. Ariawan AB, Ebnesajjad S. Hatzikiriakos SG. Paste extrusion of polytetrafluoroethylene (PTFE) fine powder resins. *Can J Chem Eng*. 2002;80:1153–1165.
5. Larson R. *Constitutive Equations for Polymer Melts and Solutions*. Boston, MA: Butterworths; 1998.
6. Hoffman O, Sachs G. *Introduction to the Theory of Plasticity for Engineers*. New York: McGraw-Hill; 1953.
7. Davis EA, Dukos J. Theory of wire drawing. *J Appl Mech*. 1994;11:193–198.
8. Benbow JJ, Oxley EW, Bridgwater J. The extrusion mechanics of pastes: The influence of paste formulation on extrusion parameters. *Chem Eng Sci*. 1987;42:2151–2162.
9. Benbow JJ, Bridgwater J. The influence of formulation on extrudate structure and strength. *Chem Eng Sci*. 1987;42:735–766.
10. Benbow JJ, Lawson TA, Oxley EW, Bridgwater J. Prediction of paste extrusion pressure. *Ceram Bull*. 1989;68:1821–1824.
11. Dealy JM, Wissbrun KF. *Melt Rheology and Its Role in Plastics Processing: Theory and Applications*. New York: Van Nostrand Reinhold; 1990.
12. Basterfield RA, Lawrence CJ, Adams MJ. On the interpretation of orifice extrusion data for viscoplastic materials. *Chem Eng Sci*. 2005;60:2599–2607.
13. Snelling GR, Lontz JF. Mechanism of lubricant: Extrusion of Teflon® TFE (tetrafluoroethylene) resins. *J Appl Polym Sci*. 1960;3:257–265.
14. Patil PD, Feng JJ, Hatzikiriakos SG. Constitutive modeling and flow simulations of polytetrafluoroethylene (PTFE) paste extrusion. *J Non-Newtonian Fluid Mech*. 2006;134:44–53.
15. Dunlap PN, Leal LG. Dilute polystyrene solutions in extensional flows birefringence and flow modification. *J Non-Newtonian Fluid Mech*. 1987;23:5–48.
16. Fuller GG, Rallison JM, Schmidt RL, Leal LG. The measurements of velocity gradients in laminar flow by homodyne light-scattering spectroscopy. *J Fluid Mech*. 1980;100:555–575.
17. Fuller GG, Leal LG. Flow birefringence of dilute polymer solutions in two-dimensional flows. *Rheol Acta*. 1980;19:580–600.
18. Mooney M. Explicit formulas for slip and fluidity. *J Rheol*. 1931;2:210–222.
19. Ochoa I, Hatzikiriakos SG. Polytetrafluoroethylene paste preforming: Viscosity and surface tension effects. *Powder Technol*. 2004;146:73–83.
20. Saint-Venant B. Mémoire sur l'établissement des equations différentielles des mouvements intérieurs opérés dans les corps solides ductiles. *C R Acad Sci Paris*. 1870;70:473–484.
21. Chakrabarty J. *Theory of Plasticity*. Singapore: McGraw-Hill; 1998.
22. Ludwik P. Elemente der Technologischen Mechanikqq. Berlin: Springer-Verlag; 1909.
23. Rivlin RS. Large elastic deformations of isotropic materials, Part IV: Further developments of the general theory. *Philos Trans R Soc Lond A Phys Sci*. 1948;241:379–397.
24. Rivlin RS. *Large elastic deformations. Rheology*. New York: Academic Press; 1956.
25. Macosko CW. *Rheology: Principles, Measurements, and Applications*. New York: VCH; 1994.
26. Ariawan AB, Ebnesajjad S, Hatzikiriakos SG. Preforming behavior of polytetrafluoroethylene paste. *Powder Technol*. 2001;121:249–258.
27. Ochoa I, Hatzikiriakos SG. Paste extrusion of polytetrafluoroethylene (PTFE): Surface tension and viscosity effects. *Powder Technol*. 2005;153:108–118.